Article, Author's Postprint

Platzek, Frank; Stelling, Guus; Jankowski, Jacek; Pietrzak, J. D.

Accurate vertical profiles of turbulent flow in z-layer models

Water Resources Research

Erstveröffentlichung in Water Resources Research 50 (2014), S. 2191-2211.
Für eine korrekte Zitierbarkeit ist die Seitennummerierung
der Originalveröffentlichung für jede Seite kenntlich gemacht. S. 2191

Accurate vertical profiles of turbulent flow in z-layer models

F. W. Platzek[1,2,3], G. S. Stelling[1,2], J. A. Jankowski[3], and J. D. Pietrzak[2]

[1] Deltares, Delft, Netherlands
[2] Fluid Mechanics Section, Faculty of Civil Engineering and Geosciences, Delft University of Technology, Delft, Netherlands
[3] Department of Hydraulic Engineering in Inland Areas, Federal Waterways Engineering and Research Institute, Karlsruhe, Germany

Correspondence to:
F. W. Platzek, frank.platzek@deltares.nl
Received 20 JULY 2013, Accepted 18 FEB 2014
Accepted article online 20 FEB 2014, Published online 11 MAR 2014

Three-dimensional hydrodynamic z-layer models, which are used for simulating the flow in rivers, estuaries, and oceans, suffer from an inaccurate and often discontinuous bottom shear stress representation, due to the staircase bottom. We analyze the governing equations and clearly show the cause of the inaccuracies. Based on the analysis, we present a new method that significantly reduces the errors and the grid dependency of the results. The method consists of a near-bed layer-remapping and a modified nearbed discretization of the k-Ɛ turbulence model. We demonstrate the applicability of the approach for uniform channel flow, using a schematized two-dimensional vertical model and for the flow over a bottom sill using the Delft3D modeling system.

1 Introduction

Three-dimensional (3-D) hydrodynamic models, such as UnTRIM [Casulli and Walters, 2000], SUNTANS [Fringer et al., 2006], Delfin [Ham et al., 2005], and Delft3D [Deltares, 2011], are applied to simulate the flow in rivers, oceans, estuaries and lakes, to predict flooding, aid in ship navigation and sediment management, and to study morphology and water quality. For such applications, the vertical structure of the flow—including possible stratification—is of key importance. Specifically, the river modeling community has only relatively recently started applying 3-D models to simulate the flow in bends and near hydraulic structures such as groynes or weirs [see e.g., Lane et al., 1999; Wu et al., 2000; Hardy et al., 2006; Nihei et al., 2007; Lege et al., 2007; Patzwahl et al., 2008].

For the vertical discretization in 3-D models, commonly either terrain-following σ-layers, as introduced by Phillips [1957], or strictly horizontal, geopotential z-layers are used (Figure 1). Using r-layers, the grid follows the bottom and free surface, allowing the relatively simple application of boundary conditions. However, problems with hydrostatic consistency arise when modeling the flow above steep bottom slopes, in particular for stratified flow [e.g., Mesinger, 1982; Haney, 1991; Stelling and van Kester, 1994]. Additionally, r-models provide excessive resolution in shallow areas

and the layering can even become singular with zero depth, posing difficulties in simulating wetting and drying.

Conversely, the z-layer discretization allows simple horizontal discretizations for pressure, advection, and diffusion and it efficiently handles shallow areas. However, the bottom and free-surface boundaries are represented as "staircases," see Figure 1. Even using a partial-cell or shaved-cell approach [see e.g., Adcroft et al., 1997; Pacanowski and Gnanadesikan, 1998], these boundaries cause problems. First, inadequate treatment of advection introduces implicit form drag along staircase boundaries [e.g., Beckmann and Döscher, 1997; Song and Chao, 2000; Chen, 2004; Ezer and Mellor, 2004; Kleptsova et al., 2010]. Second, thin layers—occurring when the bottom or free surface crosses a layer interface—cause discontinuities in velocity and shear stress, see Figure 1. Wilcox [1993] reported this problem for nonuniform grid spacing near boundaries, i.e., also for r-models. These problems were considered, e.g., by Stelling [1995]; Bijvelds [2001]; Tseng and Ferziger [2003]; and Chen [2004], but we did not find proof that the proposed approaches provide accurate results on relatively coarse, nonuniform grids, when combined with a sophisticated vertical turbulence model.

Similar considerations hold for immersed boundary methods (IBMs). In such methods, the boundary arbitrarily cuts through the grid, forming an immersed boundary. The effect of this boundary on the flow can then be incorporated in the governing equations in a number of ways. One common approach is to use ghostcells, situated outside the boundary. The boundary condition is then transferred from the actual boundary to the ghost cell using interpolation [Tseng and Ferziger, 2003; Mittal and Iaccarino, 2005]. Another approach

Platzek, Stelling, Jankowski, Pietrzak: Accurate vertical profiles of turbulent flow in z-layer models
Water Resources Research (2014), S. 2191-2211. S. 2192

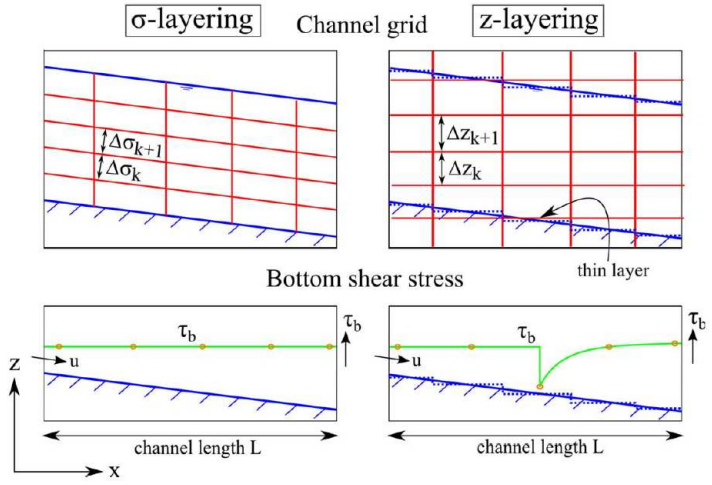

Figure 1. Vertical grid structure and bottom shear stress for uniform channel flow, using (left) the r-layer grid and (right) the z-layer grid.

is to apply cut-cells, where large ratios in cell size can occur near the boundary. This problem is very similar to the problem of thin layers in z-layer models. In IBMs, the small-cells problem was addressed, e.g., by Kirkpatrick et al. [2003] and Seo and Mittal [2011].

Specifically for fluvial applications, the application of z-layers offers a considerable decrease in computational time, due to the efficient treatment of shallow (floodplain) areas, using a limited number of layers. However, the resistance effect of the bottom boundary layer in these shallow areas—also over variable topography—must be adequately represented using the relatively coarse vertical resolution. This is a known problem for z-layer models and severely limits the application of these models, especially in combination with morphodynamics. We therefore aim at accurate representation of bottom shear stress and vertical shear in z-layers, specifically with limited grid resolution.

We first give a general description of the 3-D models to which this work applies. We then identify the cause of the erroneous variation of the bottom shear stress and velocity in z-layer models with a staircase bottom, by analyzing a schematic one-dimensional vertical (1-DV) model with an algebraic turbulence model, applicable to uniform channel flow. From this analysis, we propose a near-bottom layer-remapping that significantly reduces the discretization errors that cause the erroneous variation.

Additionally, based on numerical experiments with the k-ε turbulence model, we present a modified near-bottom discretization of the vertical diffusion terms in the k-ε turbulence model. We test the methods for uniform channel flow using a width-averaged 2-D vertical (2-DV) model and for the flow over a bottom sill using the Delft3D modeling system, both using the k-ε turbulence model. We show that the dependency of the results on the near-bed grid structure in z-layer models is greatly reduced and the accuracy of the vertical profiles greatly improved using the new method.

2 Mathematical Model

We consider a 3-D z-layermodel, applicable tomodeling rivers, estuaries, andoceans, as, e.g., UnTRIM [Casulli and Walters, 2000], SUNTANS [Fringer et al., 2006], Delfin [Ham et al., 2005], and Delft3D [Deltares, 2011]. These models

Platzek, Stelling, Jankowski, Pietrzak: Accurate vertical profiles of turbulent flow in z-layer models
Water Resources Research (2014), S. 2191-2211.

differ foremost in the time integration, advection scheme, and wetting and drying algorithms. For our analysis of the bottomshear stress and vertical profiles, these differences are not important. For simplicity, we assume a hydrostatic pressure, but the new methods presented in this paper also apply to nonhydrostaticmodels.

2.1 Continuous Model

The 3-D model consists of the momentum equations in x and y directions (omitting buoyancy for simplicity):

$$\frac{\partial u}{\partial t}+u\frac{\partial u}{\partial x}+v\frac{\partial u}{\partial y}+w\frac{\partial u}{\partial z}-fv=-g\frac{\partial \zeta}{\partial x}+\frac{\partial}{\partial x}\left(\nu_h\frac{\partial u}{\partial x}\right)+\frac{\partial}{\partial y}\left(\nu_h\frac{\partial u}{\partial y}\right)+\frac{\partial}{\partial z}\left(\nu\frac{\partial u}{\partial z}\right) \tag{1}$$

$$\frac{\partial v}{\partial t}+u\frac{\partial v}{\partial x}+v\frac{\partial v}{\partial y}+w\frac{\partial v}{\partial z}+fu=-g\frac{\partial \zeta}{\partial y}+\frac{\partial}{\partial x}\left(\nu_h\frac{\partial v}{\partial x}\right)+\frac{\partial}{\partial y}\left(\nu_h\frac{\partial v}{\partial y}\right)+\frac{\partial}{\partial z}\left(\nu\frac{\partial v}{\partial z}\right) \tag{2}$$

where u, v, and w are the velocity components in x, y, and z directions, respectively, t represents time, ζ is the free-surface level, ν_h and ν are the horizontal and vertical eddy viscosities, f is the Coriolis parameter, and g is the gravitational acceleration. We note that commonly ν refers to the molecular viscosity and ν_t to the turbulent eddy viscosity. For brevity, we have used ν in the rest of this work.

Omitting sources for simplicity, the continuity equation reads:

$$\frac{\partial u}{\partial x}+\frac{\partial v}{\partial y}+\frac{\partial w}{\partial z}=0 \tag{3}$$

After vertical integration and using kinematic relations at the free surface and bottom, (3) can be rewritten to the free-surface equation:

$$\frac{\partial \zeta}{\partial t}+\frac{\partial}{\partial x}\left(\int_{-d}^{\zeta} u dz\right)+\frac{\partial}{\partial y}\left(\int_{-d}^{\zeta} v dz\right)=0 \tag{4}$$

where d is the bottom depth (positive downward from the reference level).

Neglecting wind shear, the bottom and free-surface boundary conditions for (1) and (2) are

$$\nu \frac{\partial u}{\partial z}\Big|_{z=-d} = |U_*| u_*, \quad \nu \frac{\partial v}{\partial z}\Big|_{z=-d} = |U_*| v_* \tag{5}$$

$$\nu \frac{\partial u}{\partial z}\Big|_{z=\zeta} = 0, \quad \nu \frac{\partial v}{\partial z}\Big|_{z=\zeta} = 0 \tag{6}$$

where u_* and v_* are the shear velocities, which can be determined, e.g., based on a Chézy or Manning formulation. We define u_* and v_* based on the assumption of the logarithmic law of the wall for fully developed turbulent flow:

$$u_* = \frac{\kappa u^+}{\ln\left(\frac{z^+}{z_0}+1\right)}, \quad v_* = \frac{\kappa v^+}{\ln\left(\frac{z^+}{z_0}+1\right)} \tag{7}$$

$$|U_*| = \frac{\kappa U^+}{\ln\left(\frac{z^+}{z_0}+1\right)} \tag{8}$$

where j is the von Kármán constant, u^+ and v^+ are velocities at a height z^+ from the bottom, $U^+=((u^+)^2+(v^+)^2)^{1/2}$, and z_0 is the roughness height, which is commonly defined as $z_0=k_s/30$, where k_s is known as Nikuradse's equivalent sand roughness. Parameter z_0 (or k_s) is often used as primary calibration parameter.

To complete the 3-D model, we need turbulence closures to compute the eddy viscosities ν_h and ν. For simplicity, we assume ν_h to be constant. To obtain accurate vertical profiles for a wide range of applications, we apply the standard k-Ɛ turbulence model [Jones and Launder, 1972] to compute the vertical eddy viscosity ν. For the model to be numerically stable, it is essential that ν is strictly positive. Mohammadi and Pironneau

Platzek, Stelling, Jankowski, Pietrzak: Accurate vertical profiles of turbulent flow in z-layer models
Water Resources Research (2014), S. 2191-2211.

[1994, p. 56–57 and 65–66] show that under the assumptions made to derive the differential form of the k-Ɛ model, the model has strictly positive solutions.

In the k-Ɛ model, ν is computed from the turbulent kinetic energy k and its dissipation rate Ɛ:

$$\nu = c_\mu \frac{k^2}{\varepsilon} \tag{9}$$

where c_μ is an empirical constant. The unknowns k and Ɛ are computed using two separate transport equations. The 3-D k- and Ɛ-equations read:

$$\frac{\partial k}{\partial t}+u\frac{\partial k}{\partial x}+v\frac{\partial k}{\partial y}+w\frac{\partial k}{\partial z}-\frac{\partial}{\partial z}\left(\frac{\nu}{\sigma_k}\frac{\partial k}{\partial z}\right)-P_k+\varepsilon=0 \tag{10}$$

$$\frac{\partial \varepsilon}{\partial t}+u\frac{\partial \varepsilon}{\partial x}+v\frac{\partial \varepsilon}{\partial y}+w\frac{\partial \varepsilon}{\partial z}-\frac{\partial}{\partial z}\left(\frac{\nu}{\sigma_\varepsilon}\frac{\partial \varepsilon}{\partial z}\right)-P_\varepsilon+\varepsilon_\varepsilon=0 \tag{11}$$

where

$$P_k=\nu\left[\left(\frac{\partial u}{\partial z}\right)^2+\left(\frac{\partial v}{\partial z}\right)^2\right] \tag{12}$$

$$P_\varepsilon=c_{1\varepsilon}\frac{\varepsilon}{k}P_k=c_{1\varepsilon}c_\mu k\left[\left(\frac{\partial u}{\partial z}\right)^2+\left(\frac{\partial v}{\partial z}\right)^2\right] \tag{13}$$

$$\varepsilon_\varepsilon=c_{2\varepsilon}\frac{\varepsilon^2}{k} \tag{14}$$

are the production rate of k, the production rate of Ɛ, and the dissipation rate of Ɛ, respectively. We have neglected the horizontal diffusion terms as they are commonly very small compared to the other terms [Bijvelds, 2001] and also because the advection terms will be discretized using the dissipative (but stable and positive) first-order upwind scheme. Adding the horizontal diffusion terms would lead to excessive horizontal dissipation [van Kester, 1994].

In the absence of wind shear, Dirichlet boundary conditions for the k-Ɛ model are [see e.g., Rodi, 1984]:

$$\begin{aligned} k|_{z=-d}&=\frac{|U_*|^2}{\sqrt{c_\mu}}, & \varepsilon|_{z=-d}&=\frac{|U_*|^3}{\kappa z_0}, & \nu|_{z=-d}&=\kappa|U_*|z_0 \\ k|_{z=\zeta}&=k_{bg}, & \varepsilon|_{z=\zeta}&=\varepsilon_{bg}, & \nu|_{z=\zeta}&=\nu_{bg} \end{aligned} \tag{15}$$

where k_{bg}, ε_{bg}, and ν_{bg} are background values that account for some background turbulence, of which we assume it is always present. The background value for v satisfies (9). In our tests, we used $k_{bg}=1{:}0e^{-5}\,m^2/s^2$, $\varepsilon_{bg}=9.0e^{-7}\,m^2=s^3$, and $\nu_{bg}=1.0e^{-5}\,m^2/s$. We also use these values as initial conditions for the k-Ɛ model.

One could also apply Neumann-type boundary conditions for k and Ɛ as, e.g., done by Burchard and Petersen [1999] and Burchard et al. [2005] (see section 6).

The constants in the k-Ɛ model are [Rodi, 1984]:

$$c_\mu = 0.09, \quad c_{1\varepsilon} = 1.44, \quad c_{2\varepsilon} = 1.92, \quad \sigma_k = 1.0, \quad \sigma_\varepsilon = 1.3 \tag{16}$$

2.2 Discretized Model

We discretize the equations on a structured C-grid (staggered positioning of variables). For simplicity, we assume a constant grid spacing Δx and Δy. Our considerations mostly concern the vertical discretizations, rendering them also applicable to curvilinear or unstructured C-grid models. We use a semi-implicit formulation as used, e.g., in UnTRIM and SUNTANS, but a combination of our method with, e.g., an ADI-type time

Platzek, Stelling, Jankowski, Pietrzak: Accurate vertical profiles of turbulent flow in z-layer models
Water Resources Research (2014), S. 2191-2211.

integration as in Delft3D is also feasible as demonstrated in section 5. The vertical eddy viscosity v is defined in w-points, i.e., at the layer interfaces. The discretized momentum and free-surface equations read:

$$\frac{u^{n+1}_{i+1/2,j,k} - u^{n}_{i+1/2,j,k}}{\Delta t} + Fu^{n}_{i+1/2,j,k} - fv^{n}_{i+1/2,j,k} = -g\frac{\zeta^{n+1}_{i+1,j} - \zeta^{n+1}_{i,j}}{\Delta x} + \frac{1}{\Delta z^{n}_{i+1/2,j,k}}\left(\nu^{n}_{i+1/2,j,k+1/2}\frac{u^{n+1}_{i+1/2,j,k+1} - u^{n+1}_{i+1/2,j,k}}{\Delta z^{n}_{i+1/2,j,k+1/2}} - \nu^{n}_{i+1/2,j,k-1/2}\frac{u^{n+1}_{i+1/2,j,k} - u^{n+1}_{i+1/2,j,k-1}}{\Delta z^{n}_{i+1/2,j,k-1/2}}\right) \tag{17}$$

$$\frac{v^{n+1}_{i,j+1/2,k} - v^{n}_{i,j+1/2,k}}{\Delta t} + Fv^{n}_{i,j+1/2,k} + fu^{n}_{i,j+1/2,k} = -g\frac{\zeta^{n+1}_{i,j+1} - \zeta^{n+1}_{i,j}}{\Delta y} + \frac{1}{\Delta z^{n}_{i,j+1/2,k}}\left(\nu^{n}_{i,j+1/2,k+1/2}\frac{v^{n+1}_{i,j+1/2,k+1} - v^{n+1}_{i,j+1/2,k}}{\Delta z^{n}_{i,j+1/2,k+1/2}} - \nu^{n}_{i,j+1/2,k-1/2}\frac{v^{n+1}_{i,j+1/2,k} - v^{n+1}_{i,j+1/2,k-1}}{\Delta z^{n}_{i,j+1/2,k-1/2}}\right) \tag{18}$$

$$\frac{\zeta^{n+1}_{i,j} - \zeta^{n}_{i,j}}{\Delta t} + \frac{1}{\Delta x}\left[\sum_{k=m_{i+1/2,j}}^{k=M^{n}_{i+1/2,j}} \Delta z^{n}_{i+1/2,j,k} u^{n+1}_{i+1/2,j,k} - \sum_{k=m_{i-1/2,j}}^{k=M^{n}_{i-1/2,j}} \Delta z^{n}_{i-1/2,j,k} u^{n+1}_{i-1/2,j,k}\right] + \frac{1}{\Delta y}\left[\sum_{k=m_{i,j+1/2}}^{k=M^{n}_{i,j+1/2}} \Delta z^{n}_{i,j+1/2,k} v^{n+1}_{i,j+1/2,k} - \sum_{k=m_{i,j-1/2}}^{k=M^{n}_{i,j-1/2}} \Delta z^{n}_{i,j-1/2,k} v^{n+1}_{i,j-1/2,k}\right] = 0 \tag{19}$$

where i, j, and k are the indices corresponding to the x direction, y direction, and z direction, m is the bottom layer index, M^n is the free-surface layer index at time level n, and F_u and F_v contain the explicitly discretized advection and horizontal diffusion terms. The advection terms can be approximated, e.g., using a conservative upwind scheme as in Kleptsova et al. [2010] or an Eulerian-Lagrangian scheme [e.g., Casulli and Cheng, 1990; Ham et al., 2006].

After computing the new free-surface levels ζ and the new horizontal velocities u and v from (17–19), the vertical velocities are computed recursively upward from the bottom, using the discrete continuity equation:

$$w^{n+1}_{i,j,k+1/2} = w^{n+1}_{i,j,k-1/2} + \frac{1}{\Delta x}\left(\Delta z^n_{i-1/2,j,k} u^{n+1}_{i-1/2,j,k} - \Delta z^n_{i+1/2,j,k} u^{n+1}_{i+1/2,j,k}\right) + \frac{1}{\Delta y}\left(\Delta z^n_{i,j-1/2,k} v^{n+1}_{i,j-1/2,k} - \Delta z^n_{i,j+1/2,k} v^{n+1}_{i,j+1/2,k}\right) \tag{20}$$

$$\text{For } k = m, m+1, \ldots, M^{n-1}$$

where the vertical velocity at the botton $w^{n+1}_{i,j,m-1/2}$ is zero.

The bottom and free-surface boundary conditions for (17) and (18) are given by (again neglecting wind shear):

$$\nu^n_{i+1/2,j,m-1/2} \frac{u^{n+1}_{i+1/2,j,m} - u^{n+1}_{i+1/2,j,m-1}}{\Delta z^n_{i+1/2,j,m-1/2}} = |U_*| u_* = r_x |U^n_{i+1/2,j,m}| u^{n+1}_{i+1/2,j,m} \tag{21}$$

$$\nu^n_{i,j+1/2,m-1/2} \frac{v^{n+1}_{i,j+1/2,m} - v^{n+1}_{i,j+1/2,m-1}}{\Delta z^n_{i,j+1/2,m-1/2}} = |V_*| v_* = r_y |V^n_{i,j+1/2,m}| v^{n+1}_{i,j+1/2,m} \tag{22}$$

$$\nu^n_{i+1/2,j,M^n+1/2} \frac{u^{n+1}_{i+1/2,j,M^n+1} - u^{n+1}_{i+1/2,j,M^n}}{\Delta z^n_{i+1/2,j,M^n+1/2}} = 0 \tag{23}$$

$$\nu^n_{i,j+1/2,M^n+1/2} \frac{v^{n+1}_{i,j+1/2,M^n+1} - v^{n+1}_{i,j+1/2,M^n}}{\Delta z^n_{i,j+1/2,M^n+1/2}} = 0 \tag{24}$$

where r_x and r_y are the Taylor coefficients, which we determine from the logarithmic law of the wall:

Platzek, Stelling, Jankowski, Pietrzak: Accurate vertical profiles of turbulent flow in z-layer models
Water Resources Research (2014), S. 2191-2211.
S. 2196

$$r_x = \frac{\kappa^2}{\ln^2\left(\frac{\Delta z^n_{i+1/2,j,m}}{2z_0}+1\right)} \tag{25}$$

$$r_y = \frac{\kappa^2}{\ln^2\left(\frac{\Delta z^n_{i,j+1/2,m}}{2z_0}+1\right)} \tag{26}$$

and where

$$U^n_{i+1/2,j,m}| = \sqrt{\left(u^n_{i+1/2,j,m}\right)^2 + \left(v^n_{i+1/2,j,m}\right)^2} \tag{27}$$

$$|V^n_{i,j+1/2,m}| = \sqrt{\left(u^n_{i,j+1/2,m}\right)^2 + \left(v^n_{i,j+1/2,m}\right)^2} \tag{28}$$

Equations (25) and (26) follow when u^+ and v^+ are taken as the velocities in the bottom layer, i.e., at $z^+ = \Delta z^n_m/2$, in (7). We note that—in contrast to (8)—due to the staggering, $|U_*|_j$ and $|V_*|$ are now different, because they concern absolute velocities in different positions on the grid.

The model is completed by the discretized k-Ɛ turbulence model. We define k and Ɛ at the layer interfaces, in correspondence with v. The placement of v at the layer interfaces avoids vertical averaging of the viscosity in the horizontal momentum equations (17) and (18), but instead requires such averaging in the k- and Ɛ-equations. This leads to inaccuracies, specifically near the bottom (see section 4).

To maintain positive solutions for k and Ɛ, we use Patankar's linearization of the sink terms in the k- and Ɛ-equations [Patankar, 1980]. This linearization can be justified as follows. The dissipation Ɛ is defined as $\varepsilon = k^{3/2}/l_t = \sqrt{k}k/l_t$, where lt is a turbulent length scale. In writing an expression for ε^{n+1}, this form suggests a linearization like Patankar's:

The discrete k-Ɛ model then reads:

$$\varepsilon^{n+1} = \frac{\sqrt{k^n}k^{n+1}}{l^n_t} = \frac{\varepsilon^n k^{n+1}}{k^n} \tag{29}$$

$$\frac{k^{n+1}_{i,j,k+1/2}-k^{n}_{i,j,k+1/2}}{\Delta t}+Fk^{n}_{i,j,k+1/2} \quad -\frac{1}{\Delta z^{n}_{i,j,k+1/2}}\left(\frac{\nu^{n}_{i,j,k+1}}{\sigma_k}\frac{k^{n+1}_{i,j,k+3/2}-k^{n+1}_{i,j,k+1/2}}{\Delta z^{n}_{i,j,k+1}}-\frac{\nu^{n}_{i,j,k}}{\sigma_k}\frac{k^{n+1}_{i,j,k+1/2}-k^{n+1}_{i,j,k-1/2}}{\Delta z^{n}_{i,j,k}}\right)$$
$$-(P_k)_{i,j,k+1/2}+\underbrace{\frac{k^{n+1}_{i,j,k+1/2}}{k^{n}_{i,j,k+1/2}}\varepsilon^{n}_{i,j,k+1/2}}_{\text{Patankar's linearization}}=0 \tag{30}$$

$$\frac{\varepsilon^{n+1}_{i,j,k+1/2}-\varepsilon^{n}_{i,j,k+1/2}}{\Delta t}+F\varepsilon^{n}_{i,j,k+1/2} \quad -\frac{1}{\Delta z^{n}_{i,j,k+1/2}}\left(\frac{\nu^{n}_{i,j,k+1}}{\sigma_\varepsilon}\frac{\varepsilon^{n+1}_{i,j,k+3/2}-\varepsilon^{n+1}_{i,j,k+1/2}}{\Delta z^{n}_{i,j,k+1}}-\frac{\nu^{n}_{i,j,k}}{\sigma_\varepsilon}\frac{\varepsilon^{n+1}_{i,j,k+1/2}-\varepsilon^{n+1}_{i,j,k-1/2}}{\Delta z^{n}_{i,j,k}}\right)$$
$$-c_{1\varepsilon}\frac{\varepsilon^{n}_{i,j,k+1/2}}{k^{n}_{i,j,k+1/2}}(P_k)_{i,j,k+1/2} \quad \underbrace{+c_{2\varepsilon}\frac{\varepsilon^{n}_{i,j,k+1/2}}{k^{n}_{i,j,k+1/2}}\varepsilon^{n+1}_{i,j,k+1/2}}_{\text{Patankar's linearization}}=0 \tag{31}$$

where

$$\nu^{n}_{i,j,k}=\frac{\left(\nu^{n}_{i,j,k+1/2}+\nu^{n}_{i,j,k-1/2}\right)}{2} \tag{32}$$

$$(P_k)_{i,j,k+1/2}=\frac{\nu^{n}_{i,j,k+1/2}}{4}\left(\begin{array}{l}\left(\frac{u^{n}_{i-1/2,j,k+1}-u^{n}_{i-1/2,j,k}}{\Delta z^{n}_{i-1/2,j,k+1/2}}\right)^2+\left(\frac{u^{n}_{i+1/2,j,k+1}-u^{n}_{i+1/2,j,k}}{\Delta z^{n}_{i+1/2,j,k+1/2}}\right)^2\\ +\left(\frac{v^{n}_{i,j-1/2,k+1}-v^{n}_{i,j-1/2,k}}{\Delta z^{n}_{i,j-1/2,k+1/2}}\right)^2+\left(\frac{v^{n}_{i,j+1/2,k+1}-v^{n}_{i,j+1/2,k}}{\Delta z^{n}_{i,j+1/2,k+1/2}}\right)^2\end{array}\right) \tag{33}$$

and where $FK^{n}_{i,j,k+1/2}$ and $F\varepsilon^{n}_{i,j,k+1/2}$contain the advection terms, which we discretize using an explicit firstorder upwind scheme, see Bijvelds [2001].

Platzek, Stelling, Jankowski, Pietrzak: Accurate vertical profiles of turbulent flow in z-layer models
Water Resources Research (2014), S. 2191-2211. S. 2197

The boundary conditions for the k-Ɛ model (neglecting wind shear) are given by (15). After computing k and Ɛ, the eddy viscosity m is obtained from (9).

3 Influence of the Staircase Bottom

Three-dimensional z-layer models as described in section 2 suffer from an inaccurate and often discontinuous bottom shear stress representation, due to the staircase approximation of the bottom. More specifically, the discontinuities in velocities and bottom shear stress occur at locations

where the bottom crosses a layer interface, introducing a thin layer. We have analyzed the governing equations and will clearly show that the errors are caused by inaccuracy of the central discretization of the vertical diffusion term in the horizontal momentum equations (17) and (18), near the bottom.

3.1 Problem Analysis for Uniform Channel Flow

To identify the cause of the inaccuracies and discontinuities in bottom shear stress and vertical profiles of horizontal velocity in z-layer models, we consider uniform channel flow, for which we know the analytical solution. Omitting advection, horizontal diffusion, Coriolis, lateral effects, the transient term, and variation of the pressure gradient, the momentum equation in the x direction (17) reduces to a 1-DV model:

$$\frac{\partial}{\partial z}\left(\nu\frac{\partial u}{\partial z}\right)=g\frac{\partial \zeta}{\partial x}=-\frac{(u_*)^2}{h} \quad \text{for } 0\le z\le h \tag{34}$$

where h is the total water depth and where we have assumed the bottom to be at z=0.

For uniform channel flow, we know that m varies parabolically in the vertical as prescribed by an algebraic turbulence model based on the mixing-length concept [Prandtl, 1925]:

$$\nu(z)=\kappa u_*(z+z_0)\left(1-\frac{z}{h}\right) \tag{35}$$

The model is completed with the bottom and free-surface boundary conditions in the x direction from (5) and (6). Solving the set of equations (34) and (35) analytically leads to the well-known logarithmic velocity profile:

$$u(z)=\frac{u_*}{\kappa}\ln\left(\frac{z}{z_0}+1\right) \tag{36}$$

However, in discretizing and solving our equations we make errors, which reduce the accuracy of the solution. The size of the errors depends on the grid distribution and the existence of possible thin layers.

3.2 Discretization

We investigated to what extent the discrete problem resembles the continuous problem. For C-grids, (34) is commonly approximated as in (17):

$$\frac{1}{\Delta z_k}\left(\nu_{k+1/2}\frac{2(u_{k+1}-u_k)}{(\Delta z_{k+1}+\Delta z_k)}-\nu_{k-1/2}\frac{2(u_k-u_{k-1})}{(\Delta z_k+\Delta z_{k-1})}\right)=-\frac{(u_*)^2}{h} \tag{37}$$

Inserting the bottom boundary condition (21), yields the following expression for (37) in the layer containing the bottom (k=m). For simplicity, we assumed m=1:

$$\frac{1}{\Delta z_1}\left(\nu_{3/2}\frac{2(u_2-u_1)}{(\Delta z_2+\Delta z_b)}-(u_*)^2\right)=-\frac{(u_*)^2}{h} \tag{38}$$

where $\Delta z_b=\Delta z_1$ is the thickness of the layer containing the bottom. For a relatively smooth bed—as can be assumed for uniform channel flow—in principle, a no-slip boundary condition could be applied at the

Platzek, Stelling, Jankowski, Pietrzak: Accurate vertical profiles of turbulent flow in z-layer models
Water Resources Research (2014), S. 2191-2211.
S. 2198

bottom. This, however, requires extreme vertical resolutions to accurately represent the boundary layer (see section 6).

From (38)—evaluating $v_{3/2}$ using (35)—we obtain an expression for u_2:

$$u_2=u_1+\frac{u_*}{\kappa}\frac{(\Delta z_2+\Delta z_b)}{2(\Delta z_b+z_0)} \tag{39}$$

which can be verified to be equal to:

$$u_2=u_1+\Delta z_{3/2}\frac{\tau_{3/2}}{\nu_{3/2}}=u_1+\Delta z_{3/2}\left(\frac{\partial u}{\partial z}\right)_{3/2} \tag{40}$$

where $\tau=\partial/\partial z$ is the shear stress. In other words, the velocity in the second layer from the bed is computed using a linear approximation of the vertical gradient in horizontal velocity at the interface between the two near-bed layers.

The near-bottom velocity u_1 is obtained by evaluating the law of the wall at the height of the first velocity point above the bottom:

$$u_1=\frac{u_*}{\kappa}\ln\left(\frac{\Delta z_b}{2z_0}+1\right) \tag{41}$$

which exactly corresponds to the analytical logarithmic solution given by (36). If the velocity approximation in (39) contains errors, these errors must therefore come from the linear approximation of the vertical velocity gradients, which vary as $\partial u/\partial z \sim \partial/\partial z(\ln(z))=1/z$.

3.3 Solution Accuracy

We investigated the accuracy of (39) and its dependency on the local grid structure, by computing the velocity profiles for I=100 different vertical grid layerings, having a constant layer thickness Δz, except for the bottom layer, which has a thickness $\Delta z/I < \Delta z_{i,b} < \Delta z$, where i is now the grid counter (see Figure 2). For this example, we chose $z_0/h=0.002$ and applied K=10 layers, in all simulations. The resulting velocity profiles for the I=100 different vertical grid distributions are given in Figure 3a.

The figure shows significant errors for those vertical grid distributions that have relatively small values of near-bed layer thickness $\Delta z_{i,b}$. The errors are particularly large near the bottom, but the effect is clearly noticeable over the complete water column. It suggests that this local error is responsible for the overall inaccuracy. Due to the fact that we used the analytical solution for u_1, the solution error of u_2 is precisely the local truncation error $\tilde{e}$ in the second layer from the bottom:

$$\tilde{e}_{i,2} = u_{i,2}^{analytic} - u_{i,2}^{numeric} \tag{42}$$

or using (36), (41), and (39):

$$\tilde{e}_{i,2} = \frac{u_*}{\kappa}\left[\ln\left(\frac{2\Delta z_{i,b}+\Delta z+2z_0}{\Delta z_{i,b}+2z_0}\right) - \frac{\Delta z+\Delta z_{i,b}}{2\left(\Delta z_{i,b}+z_0\right)}\right] \tag{43}$$

We see that $\tilde{e}_{i,2}$ depends on the layer thickness of the two near-bed layers, on u_* and on z_0. We can gain more insight in the behavior of $\tilde{e}_{i,2}$ by defining the sum of the two near-bed layer thicknesses $\overline{\Delta z}_{i,b}=\Delta z_{i,b}+\Delta z$ and by writing $\Delta z_{i,b}=\alpha\overline{\Delta z}_{i,b}=\alpha/(1-\alpha)\Delta z$ and $z_0=\beta\overline{\Delta z}_{i,b}$. Substituting these expressions in (43), we obtain:

Platzek, Stelling, Jankowski, Pietrzak: Accurate vertical profiles of turbulent flow in z-layer models
Water Resources Research (2014), S. 2191-2211.
S. 2199

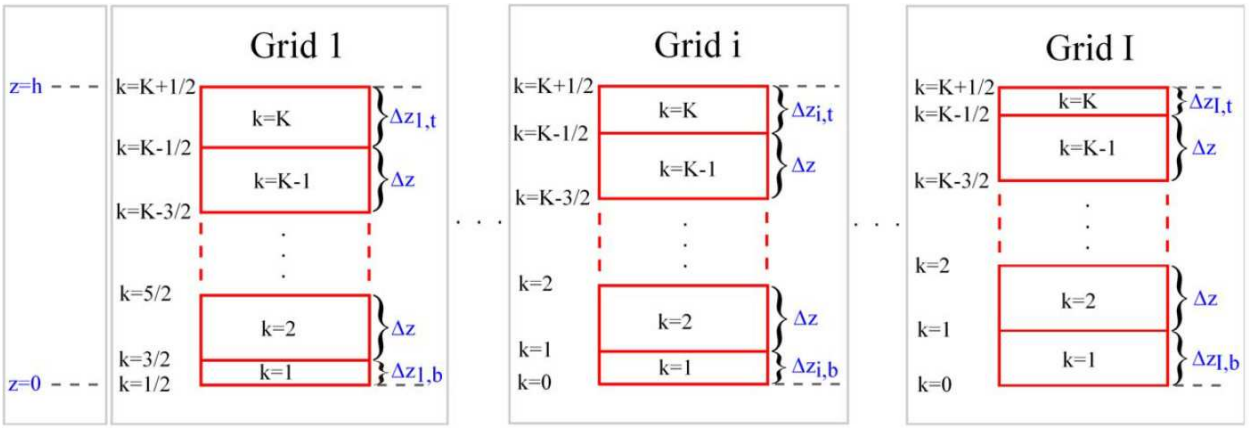

Figure 2. Three different vertical grid distributions for the 1-DV example, where all layers have thickness Δz, except for the layers containing the bottom or free surface.

$$\tilde{e}_{i,2} = \frac{u_*}{\kappa}\left[\ln\left(\frac{1+\alpha+2\beta}{\alpha+2\beta}\right) - \frac{1}{2(\alpha+\beta)}\right] \tag{44}$$

In Figure 4a, we have plotted the dimensionless, absolute percentual error ($100\,|\,\kappa\tilde{e}_{i,2}/u$) for grid distributions ranging from relatively thin near-bed layers to relatively thick near-bed layers ($0<\alpha<1$) and for the range from coarse vertical resolutions to fine vertical resolutions . When $\beta \uparrow 1$, we have a very fine vertical resolution $(\overline{\Delta z}_{i,b} \approx z_0)$ and when $\beta \downarrow 0$, we have a coarse vertical resolution $(\overline{\Delta z}_{i,b} \gg z_0)$. Since most applications have limited vertical resolution, we included a detail plot in Figure 4b, showing the error for small values of β. Several conclusions can be drawn from the figure:

1. For $0.4 \le a \le 0.5$, the error is smallest, with limited dependency on β.
2. For α smaller than $\alpha \approx 0.3$, the error grows very rapidly (in absolute sense) for coarse vertical resolutions.
3. Even for moderately fine vertical resolutions, e.g., $\beta = 0.2$ $(\overline{\Delta z}_{i,b}=5z_0)$, the error is significant for small α, i.e., for large ratios in near-bed layer thickness.

To obtain small discretization errors for a large range of a, we would require very high vertical resolution $(\overline{\Delta z}_{i,b} <\sim 2z_0)$, which we consider not feasible. We therefore investigate the option of modifying the grid near the bottom to obtain an α that provides small discretization errors in the velocity approximation, for a large range of β, i.e., both for coarse and fine vertical resolutions. To obtain $0.4 < \alpha < 0.5$, we must modify the near-bottom layering to a layering where the bottom layer thickness $\Delta z_b=\alpha/(1-\alpha)\Delta z$ Such a local remapping/remeshing is illustrated for α=0,45 in Figure 5. The remapping ensures that no large ratios in layer thickness occur near the bottom.

We can find the locally optimal ratio α for the grid layer distribution near the bottom to obtain a zero truncation error, from the following equation:

$$\ln\left(\frac{1+\alpha+2\beta}{\alpha+2\beta}\right) - \frac{1}{2(\alpha+\beta)} = 0 \tag{45}$$

which is easily solved by Newton iteration.

Figure 3b shows the drastic improvement of the results, when we use the optimal α with $\tilde{e}_{i,2}=0$ ($\alpha \approx 0.402$ for $z_0/h= 0.002$) to modify thw near-bed layer thickness to $\Delta z'_{i,b}=\alpha(\Delta z_{i,b} + \Delta z)$. The velocity profiles are very similar to the analytical solution and show almost no dependency on the grid structure.We can conclude that reducing the discretization error in the second layer from the bottom, improves the complete vertical profile.

One might suggest avoiding modification of the mesh and attempting to improve the approximation of the near-bed velocity gradients using higher order approximations. We did not pursue this, for a

number of reasons. First, we focus on coarse grids, limiting the application of larger stencils. Second, we consider the

Platzek, Stelling, Jankowski, Pietrzak: Accurate vertical profiles of turbulent flow in z-layer models
Water Resources Research (2014), S. 2191-2211.
S. 2200

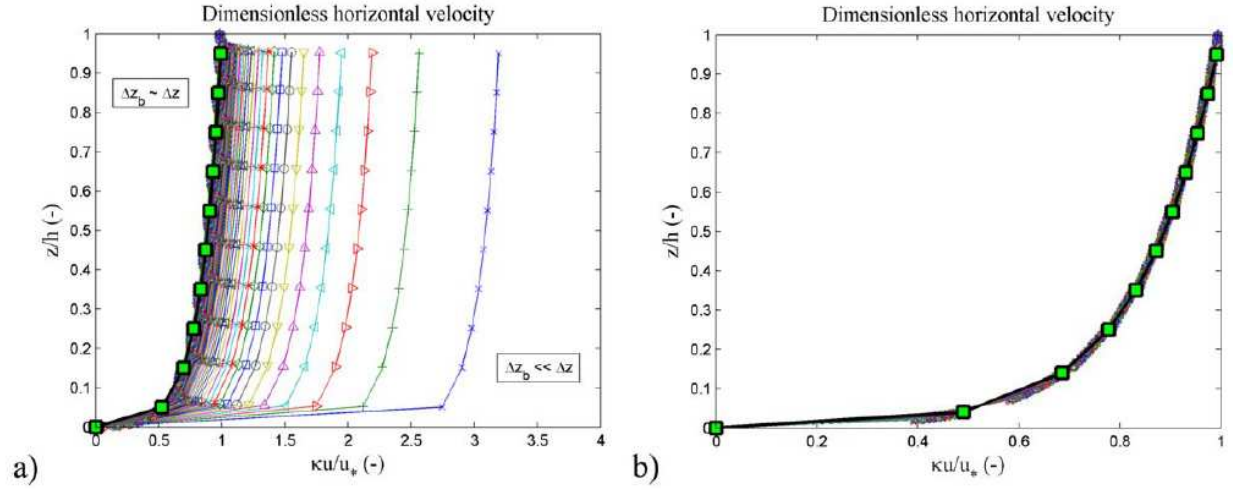

Figure 3. Dimensionless velocity profiles obtained for the 1-DV model with algebraic turbulence model, for the I=100 different vertical grid distributions (all with K=10 layers). (a) Original layering and (b) near-bed layering modified to minimize the local truncation error (α=0.402 in this case). The analytical solution is included as the thick black line with green square markers. Note the different velocity scales.

boundary layer, where the solution varies strongly, reducing the applicability of higher order schemes. And third, higher order methods only provide more accurate results on smooth grids [Hoffman, 1982]. The use of higher order discretizations within cells or elements, as in a finite element framework, may be worth investigating. This, however, requires the specification of higher order derivatives in the boundary conditions.

4 Accurate Profiles for the k-Ɛ Turbulence Model

In section 3, we analyzed the truncation errors when using an algebraic (mixing-length) turbulence model and demonstrated that the numerical approximation of the vertical profile of horizontal velocity is very sensitive to the vertical grid structure near the bottom. Applying the standard central scheme to approximate the vertical diffusion term, results in significant truncation errors for large ratios in near-bed layer thickness. The errors can be greatly reduced by remapping the two near-

bed layers using an optimal layer thickness ratio α obtained from (45). Here we demonstrate that to obtain accurate vertical profiles using the more widely applicable k-Ɛ turbulence model, the near-bed discretization of the vertical diffusion terms in the k- and Ɛ-equations requires careful attention.

4.1 Solution Accuracy for the k-Ɛ Turbulence Model

Using the reduced 1-DV model, presented in section 3, but now coupled to the k-Ɛ model to compute v, we computed profiles of u, v, k, and Ɛ for the 100 different 1-D vertical grid layerings (section 3.2). The profiles are depicted in Figure 6 (all with K=10 layers), showing the effect of the near-bed vertical layering. In the figure, we included profiles obtained using a model with K=1000 layers, as a reference solution. From the figure, we notice that the negative effect of the large ratios in near-bed layer thickness is slightly less pronounced for the 1-DV k-Ɛ model than for the algebraic turbulence model, but variability of the profiles is still clearly visible. The reduced effect can be attributed to the fact that the eddy viscosity is now coupled to the velocity and therefore also acts upon the strong velocity gradients that emerge due to the large truncation errors, i.e., the errors are smoothed out.

4.2 Improved Discretization for the k-Ɛ Turbulence Model

For the model with mixing-length turbulence, we found that modifying the near-bed layering using α=0.4-0.5, could minimize the truncation error and the variation of the velocity profiles. Conversely, for the model with k-Ɛ turbulence, we found from numerical experiments that using a near-bed equidistant layering (α=0.5), leads to the smallest dependency of the results on the grid layering. We attribute this to the $\partial Ɛ/\partial z$-term in the Ɛ-equation and the $(\partial u/\partial z)^2$-terms in the production terms in both the k- and Ɛ-equations. In the bottom boundary layer, these terms are (theoretically) proportional to $1/(z+z_0)^2$, which becomes large for thin bottom layers and moreover, the discrete (linear) approximations of these terms become inaccurate for large ratios in near-bed layer thickness. These discrete approximations show the

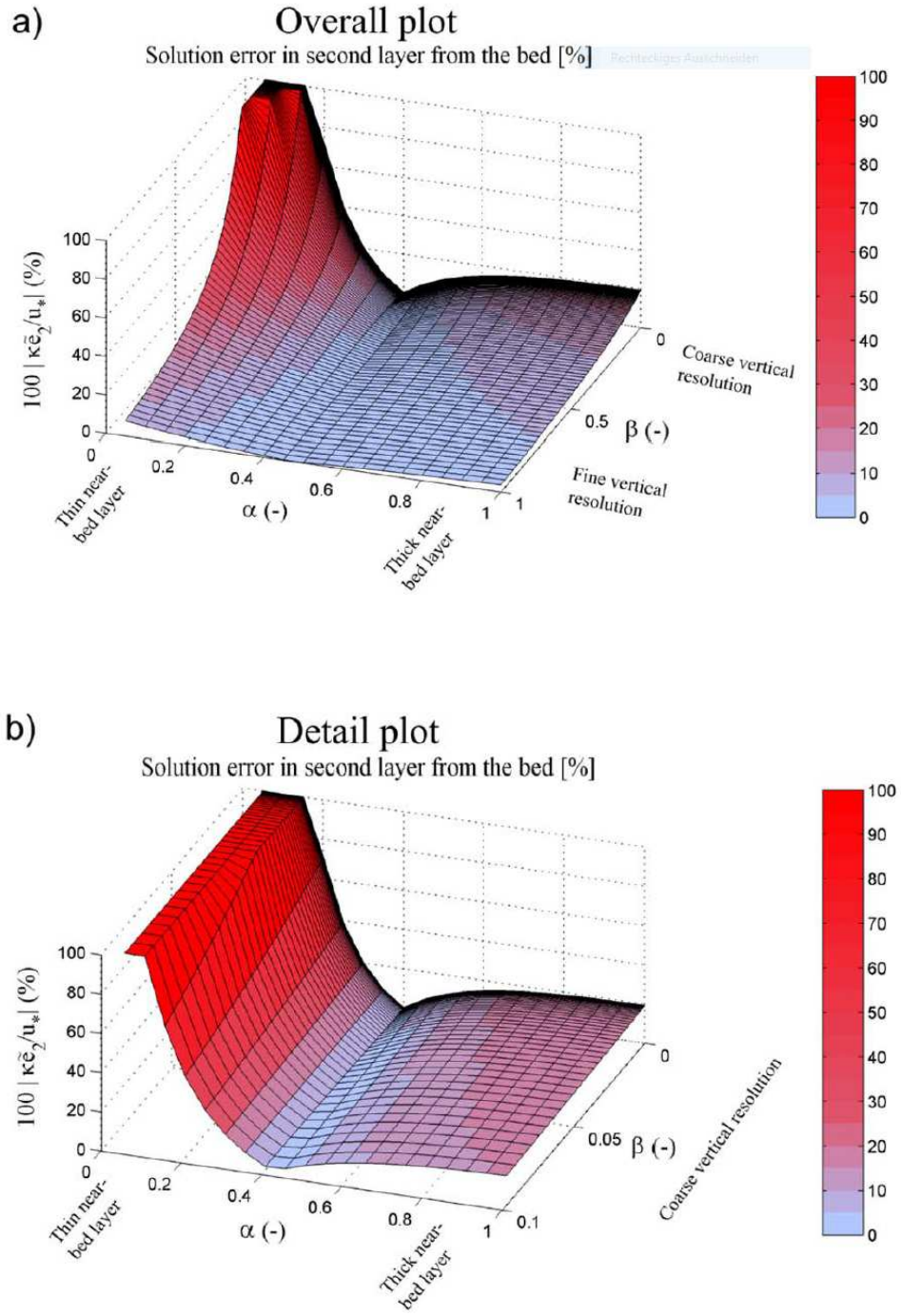

Figure 4. Percentual, absolute, dimensionless local solution error $100|\kappa\tilde{e}_{i,2}/u_*|$ as a function of near-bed layer-thickness ratio $\alpha = \Delta z_{i,b}/\overline{\Delta z}_{i,b}$ and "roughness height ratio" $\beta = z_0/\overline{\Delta z}_{i,b}$ (a) Overall plot for range $0 < \alpha < 1$ and $0 < \beta < 1$ and (b) detail plot for $\beta < 0.1$ (coarse vertical resolution).

least sensitivity when an equidistant layering is applied near the bottom. Therefore, the remapping to a near-bed equidistant layering with $\alpha = 0.5$ is applied throughout the remaining part of this pa-

per. We stress that the near-bed layering is modified for all terms in the equations, not only for the vertical diffusion and bottom shear stress computation.

Figure 7 shows the improved profiles for u, v, k, and Ɛ, obtained using the model with k-Ɛ turbulence when a modified near-bed layer thickness $\Delta z'_{i,b} = \alpha(\Delta z_{i,b} + \Delta z)$ is used, with α=0.5 (again we chose $z_0/h=0.002$).

Our numerical experiments have shown that applying an α, computed by minimizing the local truncation error using (45) reduces the variability of u with the vertical layer distribution, but it does not lead to optimal

Platzek, Stelling, Jankowski, Pietrzak: Accurate vertical profiles of turbulent flow in z-layer models
Water Resources Research (2014), S. 2191-2211.

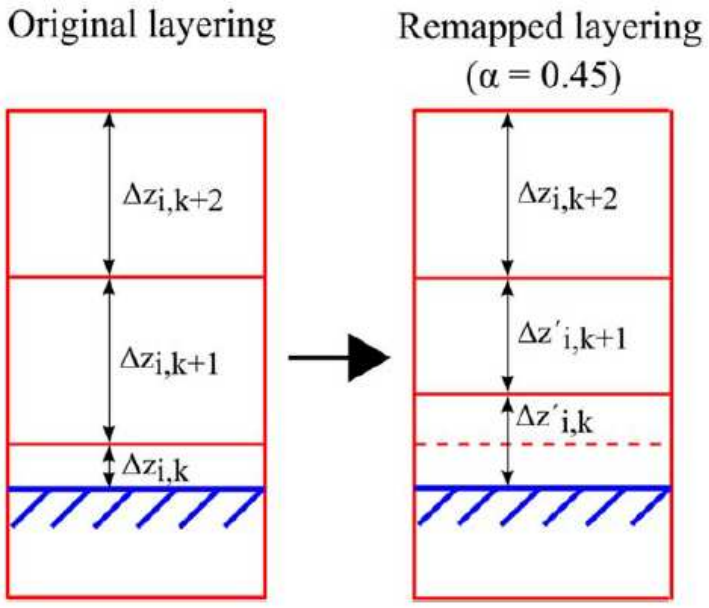

Figure 5. Remapping of the two near-bed layers to a layering with α=0.45 in a 1-DV grid.

results. This can be understood, considering that the k - Ɛ model does not lead to the "analytical" profiles for u and v (valid for the mixing-length model) and also that the vertical diffusion term of Ɛ and the production terms in both the k- and Ɛ-equations show the near-singular behavior near the bottom, described above.

Due to the described behavior of the aforementioned terms, the specification of the Dirichlet boundary conditions (15) in the k-Ɛ model is often not sufficient. For this reason, many researchers have turned to Neumann-type boundary conditions, e.g., Burchard and Petersen [1999]. We like to

maintain the Dirichlet conditions, but note that it is important that the computed near-bottom vertical diffusion fluxes in the k- and Ɛ-equations have adequate values. This should also be the case for coarse vertical discretizations, where the boundary layer is only one cell thick (or less) and for nonequidistant grid layering.

Based on numerical experiments with our code, we modified the discretization of the vertical diffusion terms of k and Ɛ near the bottom. This is necessary to achieve an accurate amount of diffusion in the nearbottom (and high-gradient) part of the water column. The following modifications are most accurate and least sensitive to the grid layering (written in 3-D notation for generality):

$$\frac{\partial}{\partial z}\left(\frac{\nu}{\sigma_k}\frac{\partial k}{\partial z}\right)\Big|_{i,j,3/2}^{n+1}=\frac{1}{\Delta z_{i,j,3/2}^{n}}\left(\frac{\nu_{i,j,2}^{n}}{\sigma_k}\frac{k_{i,j,5/2}^{n+1}-k_{i,j,3/2}^{n+1}}{\Delta z_{i,j,2}^{n}}-\frac{\nu_{i,j,3/2}^{n}}{\sigma_k}\frac{k_{i,j,3/2}^{n+1}-k_{i,j,1/2}^{n+1}}{\Delta z_{i,j,1}^{n}}\right) \tag{46}$$

$$\frac{\partial}{\partial z}\left(\frac{\nu}{\sigma_\varepsilon}\frac{\partial \varepsilon}{\partial z}\right)\Big|_{i,j,3/2}^{n+1}=\frac{1}{\Delta z_{i,j,3/2}^{n}}\left(\frac{\nu_{i,j,2}^{n}}{\sigma_\varepsilon}\frac{\varepsilon_{i,j,5/2}^{n+1}-\varepsilon_{i,j,3/2}^{n+1}}{\Delta Z_{i,j,2}^{n}}-\frac{\tilde{\nu}_{i,j,1}^{n}}{\sigma_\varepsilon}\frac{\varepsilon_{i,j,3/2}^{n+1}-\varepsilon_{i,j,1/2}^{n+1}}{\Delta z_{i,j,1}^{n}}\right) \tag{47}$$

Where $\nu_{i,j,2}^{n}=\left(\nu_{i,j,3/2}^{n}+\nu_{i,j,5/2}^{n}\right)/2$ and where we defined:

$$\tilde{\nu}_{i,j,1}^{n}=\frac{2\nu_{i,j,1/2}^{n}\nu_{i,j,3/2}^{n}}{\nu_{i,j,1/2}^{n}+\nu_{i,j,3/2}^{n}}, \tag{48}$$

i.e., we modified the viscosities that are used in the computation of the near-bed diffusion fluxes for k and Ɛ. For *k*, it is best to take its value at the first interface above the bottom. For Ɛ, we changed the vertical averaging of ν in the near-bottom part of the diffusion flux from a strictly arithmetic average to a harmonic average, which was also used by Deubelbeiss and Kaus [2008] for geodynamic simulations (Stokes equations) with strongly varying viscosity.

Especially for Ɛ, this is important to make sure the discretization results in an accurate near-bottom diffusion flux, also for coarse resolutions. Our numerical experiments confirmed that the combination of a locally equidistant near-bed layering with the discretizations given in (46–48) provides the least sensitive near-bed diffusion fluxes for k and Ɛ, and therefore, the most accurate velocity profiles, for a large range of vertical layer distributions. The considerations presented here also apply to σ-models, as the standard near-bottom approximation of $\nu\partial\varepsilon/\partial z$ is also inaccurate for coarse (near-)equidistant grid layering.

We have illustrated that when aiming to resolve the vertical flow structure for a uniform channel flow situation using a model with k-Ɛ turbulence, two aspects are of key importance: applying an equidistant grid layering near the bottom and adequately computing the near-bottom vertical diffusion fluxes of k and Ɛ.

Platzek, Stelling, Jankowski, Pietrzak: Accurate vertical profiles of turbulent flow in z-layer models
Water Resources Research (2014), S. 2191-2211.
S. 2203

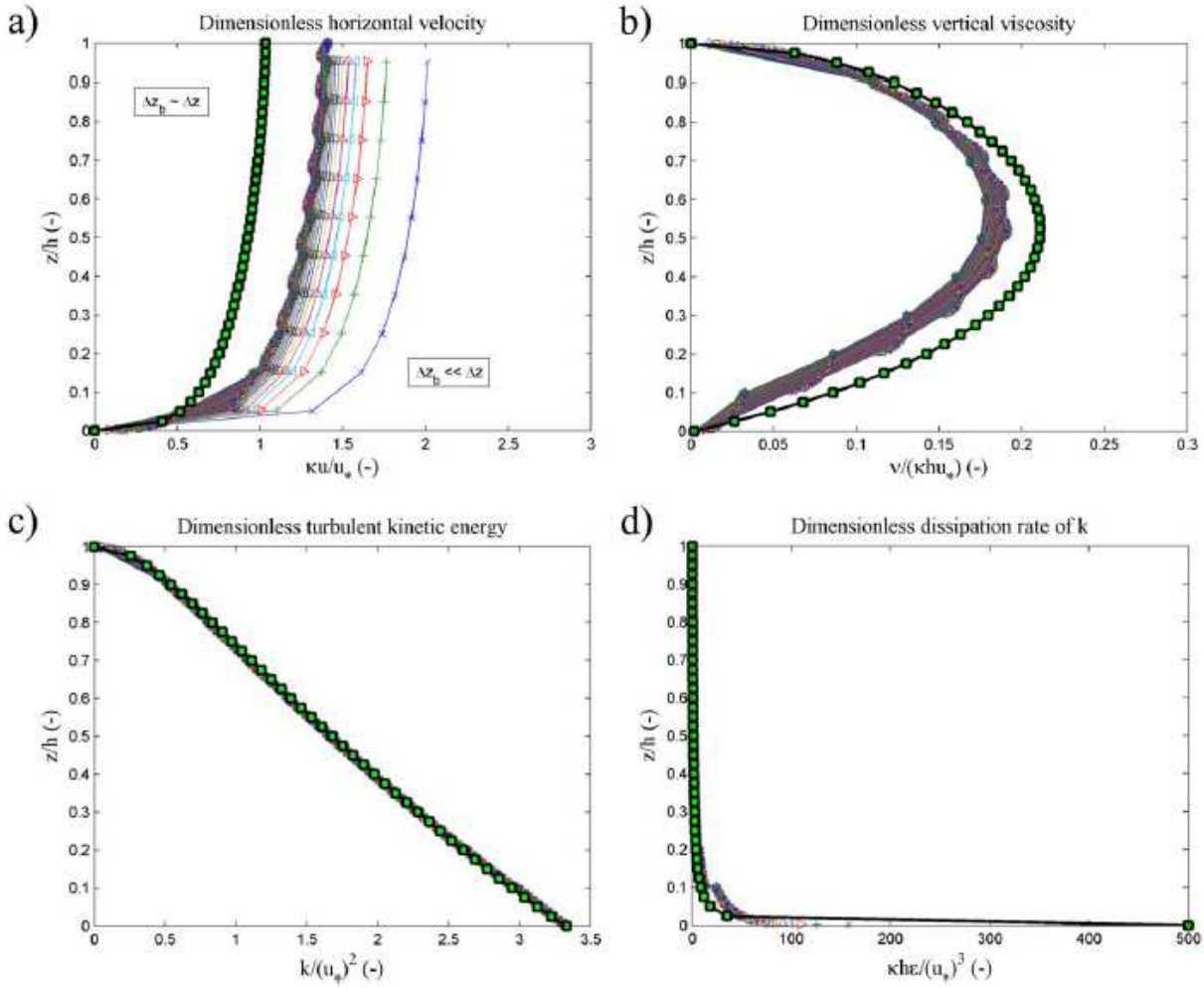

Figure 6. Dimensionless vertical profiles obtained for the uniform channel flow using the k-Ɛ turbulence model for the I=100 different vertical grid distributions (all with K=10 layers); (a) horizontal velocity u; (b) eddy viscosity ν; (c) turbulent kinetic energy k; and (d) dissipation rate Ɛ. Reference solutions using K=1000 layers are given by the thick black line with green square markers.

5 Results

In this section, we consider two models. First, a reduced 2-DV model, where we do not account for advection, horizontal diffusion, wind, buoyancy effects, and Coriolis forcing, which we use to model the uniform channel flow. Second, we use the z-layer module of Delft3D [Deltares, 2011], to model

the flow over a sinusoidal bottom sill. We compare the results with those obtained using the Delft3D σ-model.

5.1 Uniform Channel Flow

We test the 2-DV version of the schematic model described in section 3, including the k-Ɛ turbulence model. We prescribe a constant discharge per unit width q=hu at inflow and apply a Sommerfeld (or linearized Riemann) condition for the water level at the outflow boundary, converging to a steady state water level gradient at the boundary equal to the bed level gradient:

$$q|_{x=0} = q_{in} \tag{49}$$

$$\frac{\partial \zeta}{\partial t} + \sqrt{gh}\frac{\partial \zeta}{\partial x}\Big|_{x=L} = -\sqrt{gh}\, i_b \tag{50}$$

where i_b is the bottom slope (positive downward).

Platzek, Stelling, Jankowski, Pietrzak: Accurate vertical profiles of turbulent flow in z-layer models
Water Resources Research (2014), S. 2191-2211. S. 2204

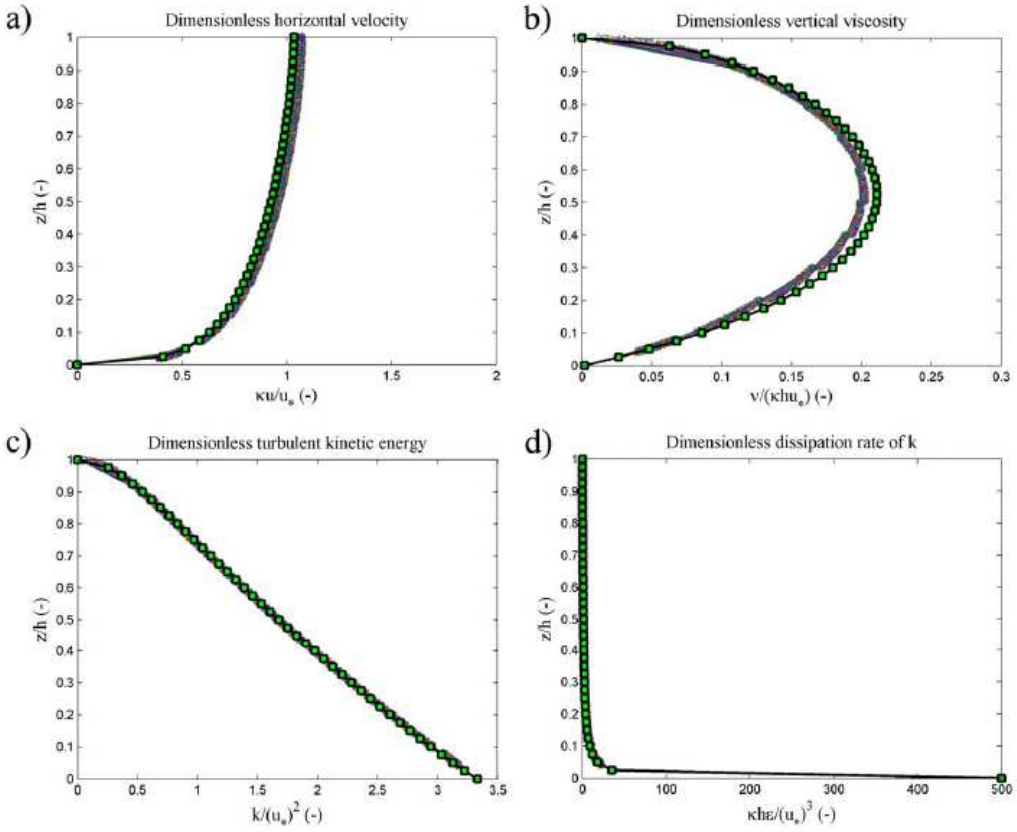

Figure 7. Dimensionless vertical profiles obtained for the uniform channel flow using the k-Ɛ turbulence model for the I=100 different vertical grid distributions, using α=0.5 to modify the layering in the two near-bed cells (all with K=10 layers); (a) horizontal velocity u; (b) eddy viscosity v; (c) turbulent kinetic energy k; and (d) dissipation rate Ɛ. Reference solutions using K=1000 layers are given by the thick black line with green square markers.

We consider a channel with length L=5000 m, i_b=0,0001 [–] and roughness height z_0=0.0023 m. As initial conditions, we set ζ=0 m and u=w=0 m/s. For the k-Ɛ model, we initialize the model with some background turbulence, to make sure that division by zero is avoided in the sink terms: $k_{bg}=1.0e^{-5} m^2/s^2$, $Ɛ_{bg}=9.0e^{-7} m^2/s^3$, and $v_{bg}=1,0e^{-5} m^2/s$. As boundary conditions, we apply $q_{in}=50 m^2/s$ at the inflow boundary and (50) for the water level at the outflow boundary.

We discretize the channel using 100 cells in x direction and 13 z-layers in z direction. All layers have a Δz=0.4 m (0,003 < β < 0:006), except for the bottom and free-surface layers, which vary in thickness along the channel due to the sloping bottom and water level. Due to the channel slope and the specific layering, the bottom crosses a layer interface once, at x=2500 m, introducing a near-bed layer thickness ratio $α=Δz_{min}/(Δz+Δz_{min})$=0,0244, where $Δz_{min}$ is the smallest allowable layer thickness in the model, which we chose to be $Δz_{min}$=0.01 m (see also section 6). This small α occurs when no layer remapping is applied.

In Figure 8, the profiles of u and v for all I=100 cells along the channel are plotted in one location. We have shifted the profiles vertically, such that the bottom lies at z=0 m. The profiles (all with K=13 layers) are shown for the original layering and for the modified near-bed layering (α=0.5), together with results obtained using K=1000 vertical layers (thick black lines with green square markers). One can see that the

velocity profiles with K=13 match the K=1000 profiles for both the original and the modified layering. The variation is now found only in the v-profiles.

The bottom shear stress $τ_b=ρ(u_*)^2$ should be constant along the channel. In Figure 9, one can see that the large near-bed layer thickness ratio introduces a discontinuity in $τ_b$. Using the proposed remapping, the variation is greatly reduced and $τ_b$ is close to the bottom shear stress obtained from the highresolution run.

For the 2-DV model, the errors due to large layer thickness ratios near the bottom express themselves differently than for the 1-DV model. For the 1-DV model, the pressure gradient is fixed and

the truncation error manifests itself in the velocity profiles, whereas for the 2-DV case, the discharge is specified from the inflow boundary condition and the truncation errors result in an erroneous bottom shear stress and equilibrium depth. The truncation error varies along the channel, growing in the direction of decreasing bottom layer thickness (upstream direction). From the downstream boundary upward, the truncation errors build up.

This can be recognized as follows: in the schematic 2-DV model, the horizontal coupling is realized through the pressure gradient and the continuity equation. Each cell has a fixed inflow from the left (equal to qin) and has a right water level which is influenced by the truncation error in the right neighbor cell and the resulting (slightly erroneous) equilibrium depth in that cell. This effect accumulates upstream causing an artificial backwater effect. At x=2500 m, the truncation error changes sign, becomes small, and then accumulates again in upstream direction.

5.2 Flow Over a Bottom Sill

To test the method for use in more general flow situations, we implemented the approach in the z-layer module of the Delft3D modeling system and simulated the flow over a bottom sill passing through a number of z-layers. We applied again the k-Ɛ turbulence model to compute v. The test concerns a 400 m long flume, with a bottom depth of 9 m (excluding the bottom sill) and an initial water level of ζ=0 m. The smooth bottom sill has a total length of 200 m (75 m sinusoidal, 50 m crest, and again 75 m sinusoidal), extends from x=20 m to x=220 m and has a height of 1.92 m. The grid is 2-DV, has 400 cells in y direction and 10 equidistant layers. At inflow a velocity of v=0.65 m/s is specified and at outflow the water level is kept fixed at ζ=0 m. We used a roughness height z_0=0.002 m. The model was completed using the default settings of the Delft3D z-layer model.

In Figure 10, we have compared the bottom shear stress along the flume obtained with the Delft3D r-model, the Delft3D z-model with original layering and the z-model with modified layering. One can see that using the modified layering, the shear stress distribution is much smoother than using the original layering. The z-layer results resemble the results obtained using the σ-model quite reasonably.

In this situation, advection also plays a role. The effects are considered in section 6. Advection was not switched off in Delft3D for this test and no special measures were taken. The results obtained with the approach presented here are very encouraging. They suggest that the accurate representation of near-bottom velocity and turbulence distributions in z-layer models for real life applications is within reach.

6 Discussion

We demonstrated that the near-bed layer-remapping and the modified discretizations for the vertical diffusion terms of k and Ɛ provide significantly improved vertical profiles (1-DV) and reduced erroneous variation and discontinuities in the bottom shear stress (2-DV or 3-D). The approaches are generally applicable to 3-D z-layer models. Using the proposed approaches, the obtained veloci-

ty profiles and bottom shear stress distributions were very similar to those one (usually) obtains using a σ-model, allowing the direct use of the bottom shear stresses for morphodynamic computations.

As mentioned in section 1, the presented considerations may also apply to immersed boundary methods (IBMs). When applying IBMs with a cut cell approach, the resulting grid has large jumps in cell size near the boundary, where a (logarithmic) boundary layer is supposed to be represented. For relatively coarse meshes

Platzek, Stelling, Jankowski, Pietrzak: Accurate vertical profiles of turbulent flow in z-layer models
Water Resources Research (2014), S. 2191-2211.

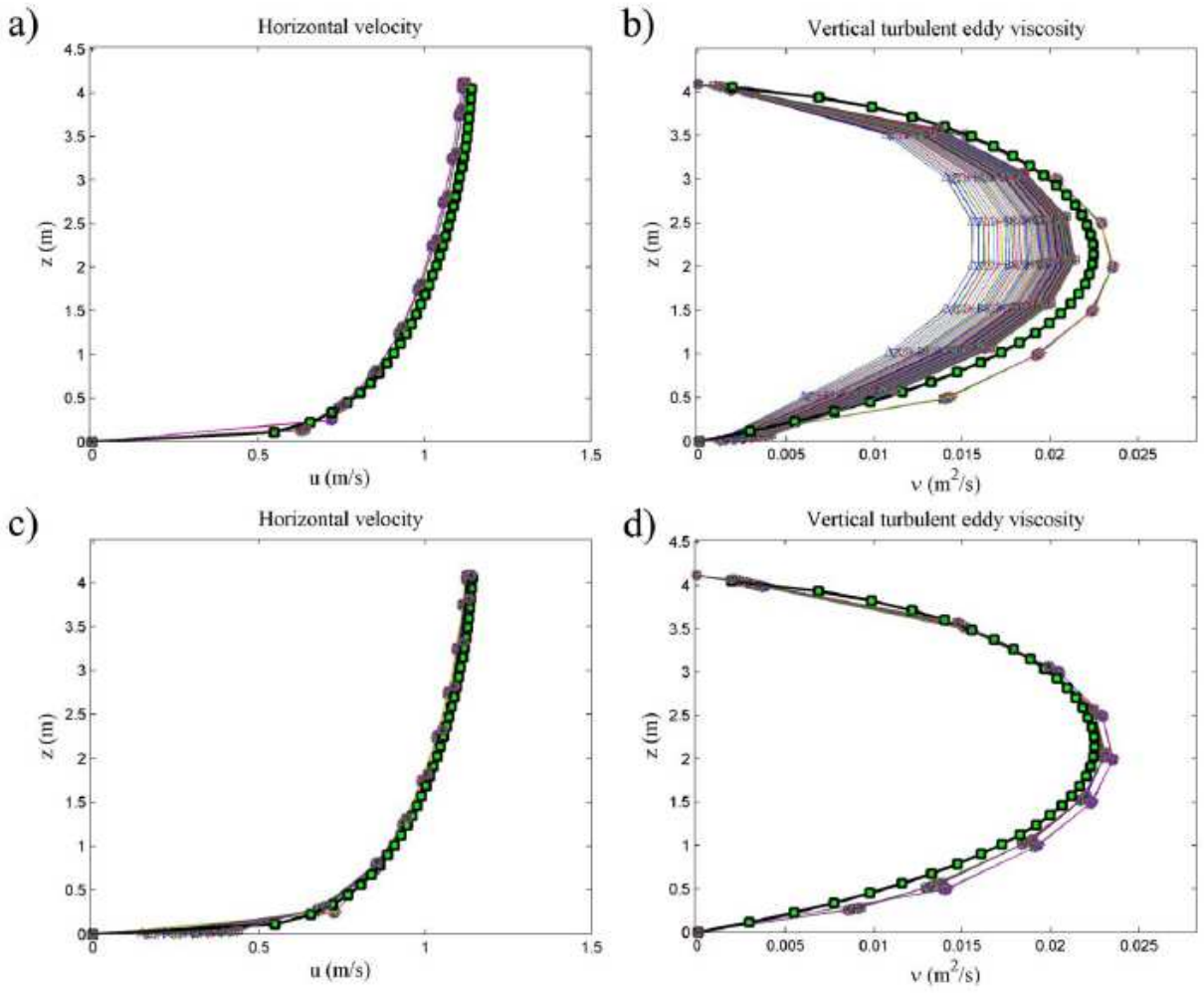

Figure 8. Vertical profiles for 2-DV uniform channel flow (all with K=13 layers); (a) horizontal velocity u using original layering; (b) vertical eddy viscosity m using original layering; (c) horizontal velocity u using modified near-bed layering; and (d) vertical eddy viscos-

ity m using modified near-bed layering. Results obtained with K=1000 layers included as the thick black lines with green square markers. Profiles have been shifted vertically such that the bottom lies at z=0 m.

(compared to the boundary layer thickness), we expect that such approaches suffer from the same problems and large discretization errors as presented here. Such methods may therefore benefit from the layerremapping approach.

When ghost-cells are applied to approximate the boundary values and the distances from the points used for interpolation to the actual boundary point vary strongly, the interpolation may be inaccurate for the same reasons as illustrated in the paper. In this case, again (locally) equidistant grids will offer most accurate results, with the least dependency on the local grid structure or interpolation stencil.

An important effect of the near-bed layer-remapping is that it causes neighbor cells to be shifted with respect to each other (see Figure 11). This should be taken into account in the computation of horizontal advection and in the possible transport of constituents. However, the remapping does not introduce problems with mass conservation, as each pair of cells uses the same cell interface area to compute the flux between the cells. The area is modified due to the remapping, but it is modified for both neighbor cells. We do not introduce multiple connectivity between cells, i.e., a cell always has only four horizontal neighbors (West, East, South, and North), with which horizontal fluxes are exchanged. Discrete volume conservation still applies:

Platzek, Stelling, Jankowski, Pietrzak: Accurate vertical profiles of turbulent flow in z-layer models
Water Resources Research (2014), S. 2191-2211. S. 2207

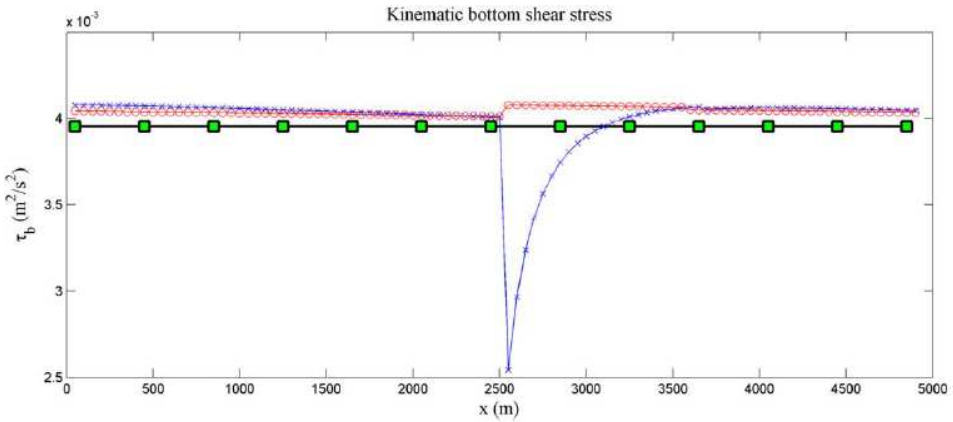

Figure 9. Shear stress variation along the channel for uniform channel flow with K=13 layers; original layering (blue line with "x"-markers), modified near-bed layering (red line

with "o"-markers) and results obtained with K=1000 layers (thick black line with green square markers)

$$\Delta x\Delta y\Delta z_{i,j,k}^{n+1} = \Delta x\Delta y\Delta z_{i,j,k}^{n} + \Delta t\Delta y\left[\Delta z_{i-1/2,j,k}^{n} u_{i-1/2,j,k}^{n+1} - \Delta z_{i+1/2,j,k}^{n} u_{i+1/2,j,k}^{n+1}\right]$$
$$+\Delta t\Delta x\left[\Delta z_{i,j-1/2,k}^{n} v_{i,j-1/2,k}^{n+1} - \Delta z_{i,j+1/2,k}^{n} v_{i,j+1/2,k}^{n+1}\right] + \Delta t\Delta x\Delta y\left[w_{i,j,k-1/2}^{n+1} - w_{i,j,k+1/2}^{n+1}\right] \quad (51)$$

even though $\Delta z_{i-1/2,j,k}$ and $\Delta z_{i,j-1/2,k}$ may not match $\Delta z_{i,j,k}$. This also applies to the transport equation.

In two specific situations, one must take special measures to maintain mass conservation. First, when the water level enters the second cell from the bottom (drying/flooding) and secondly, when the bed level changes due to morphodynamics. In such situations, we added a vertical flux at the layer interface between the two bottom layers, to account for the volume change due to $\partial\zeta/\partial t$ and $\partial d/\partial t$.This causes some spurious mixing near the bottom.

We stress that we do not alter the baricenters of the cells involved in the remapping, i.e., the baricenters of horizontal neighbors are still at the same z-level. Therefore, the remapping does not introduce spurious barotropic/ baroclinic pressure gradients.

With or without the remapping, the computation of advection over bottom steps requires attention, as, e.g., illustrated in Kleptsova et al. [2010, 2012]. Otherwise, the solution may deteriorate due to spurious form

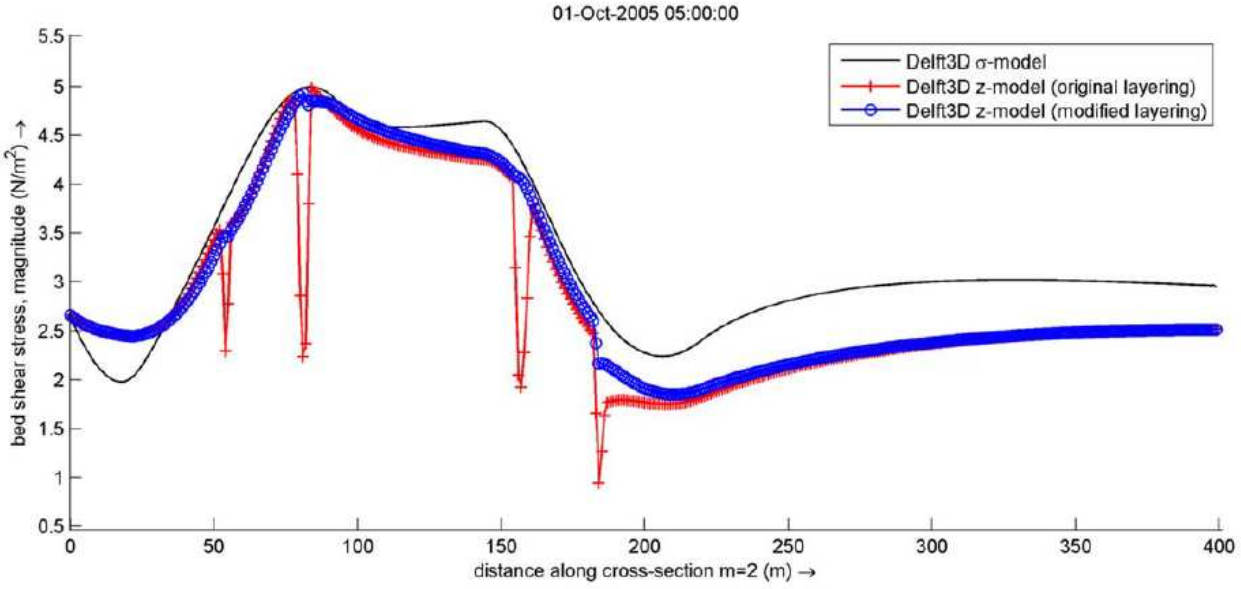

Figure 10. Bottom shear stress for the flow over a bottom sill using the Delft3D r-model (black line without markers), z-model with original layering (red line with "1"-markers), and z-model with modified layering (blue line with "o"-markers).

Platzek, Stelling, Jankowski, Pietrzak: Accurate vertical profiles of turbulent flow in z-layer models
Water Resources Research (2014), S. 2191-2211.
S. 2208

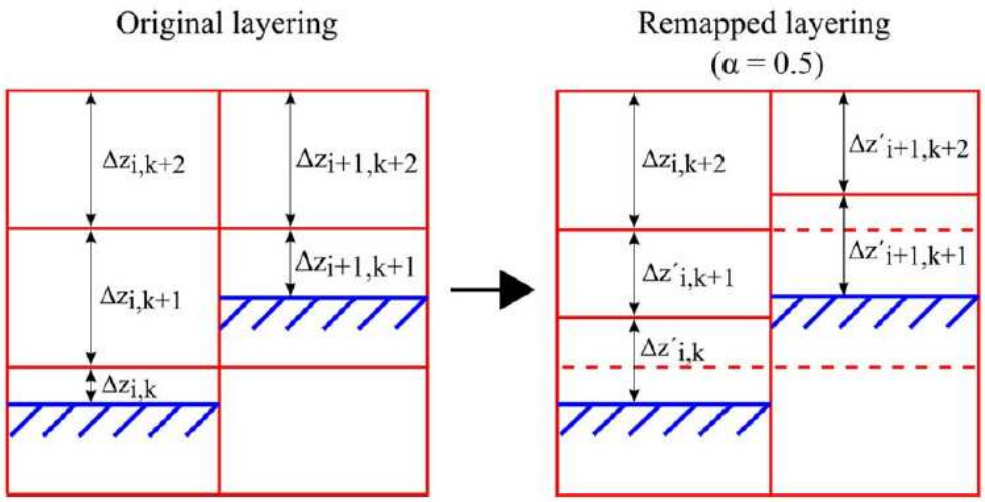

Figure 11. Remapping of the two near-bed layers to a locally equidistant layering (α=0.5) in a 2-DV grid, for cells i and i+1.

drag. The combination of our layer-remapping with the remapping proposed by Kleptsova et al. [2010] is therefore interesting to investigate. The latter remapping preserves an equidistant near-bed layering, so that no conflicts are expected in the combination. Applying an Eulerian-Lagrangian advection scheme could also be considered [e.g., Casulli and Cheng, 1990; Ham et al., 2006]. Adequate interpolation near the boundaries is then imperative.

We have inspected the vertical velocities near the bottom steps and found discontinuities, both with and without adaption of the near-bed layering. The vertical velocities in a hydrostatic model do not have an actual physical meaning, they merely serve to enforce continuity. We therefore believe that the jumps in vertical velocity might be reduced by applying a nonhydrostatic model, possibly with special care to balance the discontinuities in w near the bottom, induced by the way we commonly apply the continuity equation.

The discontinuities in vertical velocity w can probably also be reduced by applying a shaved-cell or cut-cell approach as, e.g., proposed by Adcroft et al. [1997], Kirkpatrick et al. [2003], Chen [2004],

and Seo and Mittal [2011]. Together with the layer-remapping approach and the modified near-bed discretizations in the k-Ɛ model, this may reduce the bottom-related problems in hydrodynamic z-layer models even further than shown in this paper. However, the implementation of such an approach in an existing finite difference or finite volume code is often not straightforward.

We incorporate the bottom boundary condition for the momentum equation via the law-of-the-wall approach. For a relatively smooth bed, physically, a no-slip boundary condition applies at the bottom, which should be sufficient to induce a logarithmic boundary layer profile. Unfortunately, this only holds for sufficiently high vertical resolution. Numerical experiments with the 1-DV model from section 3 have shown that even with 500 layers the velocity profiles significantly differ from (36). Assuming a logarithmic velocity profile in the bottom layer as in (41), more accurate solutions can be obtained using only five layers.

The computation of u_* from (7) requires the evaluation of the velocity at a certain height above the bed, for which we know that it is located in the logarithmic boundary layer. Commonly, this is realized by using the velocity in the lowest active grid cell $u_{i+1/2,j,m}$. However, for velocity profiles that are not (perfectly) logarithmic in the bottom boundary layer, the resulting value of u_* may be strongly dependent on the local grid structure. The grid influence is often reduced by using, e.g., the velocity in the second active layer from the bed $u_{i+1/2,j,m}$ or some weighted average of $u_{i+1/2,j,m}$ and $u_{i+1/2,j,m+1}$. By applying the equidistant near-bed layerremapping (α=0.5), the results become much less sensitive to which velocity is used for computing u_*.

Another important notice is related to the common use of a minimum layer thickness Δz_{min}. Such a parameter is often applied to avoid too thin layers in z-layer models. Both for the 2-DV and the Delft3D model, we applied Δz_{min}=0.01 m, meaning that layers that would become thinner than 0.01 m, are added to the layer above (for the bottom) or below (for the free surface). Using our layer remapping procedure, application of a Δz_{min} is strictly only necessary to avoid thin layers near the free surface, as thin layers near the bottom will get their thickness averaged with the layer above.

Platzek, Stelling, Jankowski, Pietrzak: Accurate vertical profiles of turbulent flow in z-layer models
Water Resources Research (2014), S. 2191-2211.

Applying a larger Δz_{min} would also partly relieve the problems considered in this paper. However, to obtain similar layer thickness ratios as with our remapping approach, one would have to apply Δz_{min}=0.5 Δz (with Δz a uniform or average layer thickness), which would result in the fact that near the bottom a layer would have a thickness $0{:}5\Delta z \leq \Delta z_b \leq 1{,}5\ \Delta z$. This would lead to jumps in layer thickness from 1.5 Δz to Δz for two horizontally neighboring cells, at locations where the bottom crosses a layer interface, whereas our approach results in jumps in layer thickness from Δz to 0.5 Δz for two neighboring cells. Our approach thus retains a somewhat higher resolution near the bottom.

When a $\Delta z_{min}<0.5\,\Delta z$ is applied, the layer thickness ratios and discretization errors are larger than with the remapping approach.

We apply Dirichlet boundary conditions for k and Ɛ at the bottom. Burchard and Petersen [1999] and Burchard et al. [2005] state that Neumann-type or flux-type bottom boundary conditions perform better than Dirichlet boundary conditions in many flow situations. Burchard and Petersen [1999] prescribe a zero diffusion flux for k at the bottom boundary:

$$\frac{\nu}{\sigma_k}\frac{\partial k}{\partial z}=0 \tag{52}$$

and the following relation for Ɛ:

$$\frac{\nu}{\sigma_\varepsilon}\frac{\partial \varepsilon}{\partial z}=-\left(c_\mu^0\right)^3\frac{\nu}{\sigma_\varepsilon}\frac{k^{3/2}}{\kappa\left(z+z_0\right)^2} \tag{53}$$

Where c_μ^0 is a constant. The question then remains at which height these conditions are evaluated, e.g., at the bottom interface, or at the first internal grid point, leaving an ambiguity and introducing grid dependency. The advantage of specifying Dirichlet conditions is that they are easy to implement, that the problem is well posed and that k and Ɛ are bounded.

7 Conclusions

Three-dimensional hydrodynamic z-layer models can provide erroneous velocity profiles and bottom shear stress distributions at positions where the bottom crosses a layer interface, introducing a large ratio in layer thickness near the bottom. We demonstrated this for the situation of uniform channel flow. The errors are caused by the inaccuracy of the discretization of the vertical diffusion term in the momentum equations for nonuniform vertical layering and can be avoided by performing a local remapping to an equidistant nearbed layering. The new approach works both in combination with an algebraic mixing length turbulence model and the k-Ɛ turbulence model.

Additionally, modifications in the near-bottom treatment of the vertical diffusion terms in the k- and Ɛ-equations have been presented. The combination of these modifications with the layer-remapping approach allows the accurate and smooth representation of bottom shear stress and velocity profiles along sloping channels and rivers using z-layer models. We showed the applicability using a schematic 2-D vertical model for uniform channel flow and by using the Delft3D modeling system to simulate the flow over a bottom sill. Using the new methods, it is now feasible also for z-layer models to use the straightforwardly computed bottom shear stress as direct input for coupled morphodynamic models.

Notation

α	near-bottom layer thickness ratio.
β	roughness height ratio.
Δz	layer thickness, m.
Δz_{min}	minimum allowed layer thickness, m.
ε	dissipation rate of k, m^2/s^3.
ε_ε	dissipation rate of ε, m^2/s^4.
ζ	water level, m.
K	the von Kármán constant.

Platzek, Stelling, Jankowski, Pietrzak: Accurate vertical profiles of turbulent flow in z-layer models
Water Resources Research (2014), S. 2191-2211. S. 2210

ν_h	horizontal eddy viscosity, m^2/s.
ν, ν_t	vertical eddy viscosity, m^2/s.
ρ	water density, kg/m^3.
σ_k,σ_ε	turbulent Prandtl-Schmidtnumbers for k and ε.
τ	kinematic shear stress, m^2/s^2.
$c_{1\varepsilon}$,$c_{2\varepsilon}$,c_μ,c_μ^0	constants in the k2e model.
d	bottom depth (positive downward), m.
$\tilde{e}$	local solution/truncation error.
f	Coriolis parameter, 1/s.
h	total water depth, m.
i_b	channel slope (positive downward).

I	number of 1-D vertical grids or number of horizontal grid cells (2-DV).
k	turbulent kinetic energy, m^2/s^2.
k_s	Nikuradse's equivalent sand roughness, m.
l_t	turbulent length scale, m.
L	channel length, m.
P_ε	production rate of Ɛ, m^2/s^4.
P_k	production rate of k, m^2/s^3.
q	discharge per unit width, m^2/s.
r_x	Taylor friction coefficient in x direction.
r_y	Taylor friction coefficient in y direction.
t	time, s.
u	velocity in x direction, m/s.
u_*	shear velocity in x direction, m/s.
u^+	near-bed velocity in x direction at height z^+, m/s.
v	velocity in y direction, m/s.
v_*	shear velocity in y direction, m/s.
v^+	near-bed velocity in y direction at height z^+, m/s.
w	velocity in z direction, m/s.
z_0	roughness height, m.
z^+	height above the bed where u^+ and v^+ are defined, m.

References

Adcroft, A., C. Hill, and J. Marshall (1997), Representation of topography by shaved cells in a height coordinate ocean model, Mon. Weather Rev., 125(9), 2293–2315, doi:10.1175/1520-0493(1997)125<2293:ROTBSC>2.0.CO;2.

Beckmann, A., and R. Döscher (1997), A method for improved representation of dense water spreading over topography in geopotentialcoordinate models, J. Phys. Oceanogr., 27, 581–591, doi:10.1175/1520-0485(1997)027<581:AMFIRO>2.0.CO;2.

Bijvelds, M. D. J. P. (2001), Numerical modelling of estuarine flow over steep topography, PhD thesis, Delft Univ. of Technol, Delft, Netherlands.

Burchard, H., and O. Petersen (1999), Models of turbulence in the marine environment—A comparative study of two-equation turbulence models, J. Mar. Syst., 21(1–4), 29–53, doi:10.1016/S0924-7963(99)00004-4.

Burchard, H., E. Deleersnijder, and G. Stoyan (2005), Marine turbulence: Theories, observations, and models, in Some Numerical Aspects of Turbulence-Closure Models, pp. 197–206, Cambridge Univ. Press, Cambridge, U. K.

Casulli, V., and R. T. Cheng (1990), Stability analysis of Eulerian-Lagrangian methods for the one-dimensional shallow-water equations, Appl. Math. Modell., 14, 122–131.

Casulli, V., and R. Walters (2000), An unstructured grid, three-dimensional model based on the shallow water equations, Int. J. Numer. Methods Fluids, 32(3), 331–348, doi:10.1002/(SICI)1097-0363(20000215)32:3<331::AID-FLD941>3.0.CO;2-C.

Chen, X. (2004), Using a piecewise linear bottom to fit the bed variation in a laterally averaged, z-coordinate hydrodynamic model, Int. J. Numer. Methods Fluids, 44(11), 1185–1205, doi:10.1002/fld.680.

Deltares (2011), Delft3D-FLOW: Simulation of Multi-Dimensional Hydrodynamic Flows and Transport Phenomena, Including Sediments—User Manual, Delft, Netherlands.

Deubelbeiss, Y., and B. Kaus (2008), Comparison of Eulerian and Lagrangian numerical techniques for the Stokes equations in the presence of strongly varying viscosity, Phys. Earth Planet. Inter., 171(1–4), 92–111, doi:10.1016/j.pepi.2008.06.023.

Ezer, T., and G. L. Mellor (2004), A generalized coordinate ocean model and a comparison of the bottom boundary layer dynamics in terrain-following and in z-level grids, Ocean Modell., 6(3), 379–403, doi:10.1016/s1463-5003(03)00026-x.

Fringer, O. B., M. Gerritsen, and R. L. Street (2006), An unstructured-grid, finite-volume, nonhydrostatic, parallel coastal ocean simulator, Ocean Modell., 14, 139–173, doi:10.1016/j.ocemod.2006.03.006.

Ham, D. A., J. Pietrzak, and G. S. Stelling (2005), A scalable unstructured grid 3-dimensional finite volume model for the shallow water equations, Ocean Modell., 10(1–2), 153–169, doi:10.1016/j.ocemod.2004.08.004.

Platzek, Stelling, Jankowski, Pietrzak: Accurate vertical profiles of turbulent flow in z-layer models S. 2211
Water Resources Research (2014), S. 2191-2211.

Ham, D. A., J. Pietrzak, and G. S. Stelling (2006), A streamline tracking algorithm for semi-Lagrangian advection schemes based on the analytic integration of the velocity field, J. Comput. Appl. Math., 192(1), 168–174, doi:10.1016/j.cam.2005.04.055.

Haney, R. (1991), On the pressure gradient force over steep topography in sigma coordinate ocean models, J. Phys. Oceanogr., 21, 610–619, doi:10.1175/1520-0485(1991)021<0610:OTPGFO>2.0.CO;2.

Hardy, R., D. Parsons, J. Best, S. Lane, R. Kostaschuck, and O. Orfeo (2006), Three-dimensional numerical modelling of flows over a natural dune field, in River Flow 2006, edited by E. C. T. L. Alves et al., pp. 1077–1083, Taylor and Francis, London

Hoffman, J. D. (1982), Relationship between the truncation errors of centered finite-difference approximations on uniform and nonuniform meshes, J. Comput. Phys., 46, 469–474, doi:10.1016/0021-9991(82)90028-6.

Jones, W., and B. E. Launder (1972), The prediction of laminarisation with a two-equation model of turbulence, Int. J. Heat Mass Transfer, 15, 301–314, doi:10.1016/0016/0017-9310(72)90076-2.

Kirkpatrick, M. P., S. W. Armfield, and J. H. Kent (2003), A representation of curved boundaries for the solution of the Navier-Stokes equations on a staggered three-dimensional Cartesian grid, J. Comput. Phys., 184(1), 1–36, doi:10.1016/S0021-9991(02)00013-X.

Kleptsova, O., G. Stelling, and J. Pietrzak (2010), An accurate momentum advection scheme for a z-level coordinate models, Ocean Dyn., 60(6), 1447–1461, doi:10.1007/s10236-010-0350-y.

Kleptsova, O., J. Pietrzak, and G. Stelling (2012), On a momentum conservative z-layer unstructured C-grid ocean model with flooding, Ocean Dyn., 54–55, 18–36, doi:10.1016/j.ocemod.2012.06.002.

Lane, S. N., K. F. Bradbrook, K. S. Richards, P. A. Biron, and A. G. Roy (1999), The application of computational fluid dynamics to natural river channels: Three-dimensional versus two-dimensional approaches, Geomorphology, 29(1–2), 1–20, doi:10.1016/S0169-555X(99)00003-3.

Lege, T., M. Alexy, and J. Kellermann (2007), Three-dimensional flow fields as a prerequisite for sediment transport modelling in low land rivers, in Proceedings of the 5th International Symposium on Environmental Hydraulics (ISEH V), Tempe, Ariz.

Mesinger, F. (1982), On the convergence and error problems of the calculation of the pressure gradient force in sigma coordinate models, Geophys. Astrophys. Fluid Dyn., 19, 105–117, doi:10.1080/03091928208208949.

Mittal, R., and G. Iaccarino (2005), Immersed boundary methods, Annu. Rev. Fluid Mech., 37, 239–261, doi:10.1146/annurev.fluid.37.061903.175743.

Mohammadi, B., and O. Pironneau (1994), Analysis of the k2e Turbulence Model, Wiley-Masson Ser. Res. in Appl. Math., 194 pp., John Wiley & Sons, Chichester, U. K.

Nihei, Y., Y. Kato, and K. Sato (2007), A three-dimensional numerical model for large-scale river flow with a new mode-splitting technique, paper presented at the 32nd Congress of the International Association of Hydraulic Engineering and Research, Venice, Italy.

Pacanowski, R. C., and A. Gnanadesikan (1998), Transient response in a Z-level ocean model that resolves topography with partial cells, Mon. Weather Rev., 126, 3248–3270, doi:10.1175/1520-0493(1998)126<3248:TRIAZL>2.0.CO;2.

Patankar, S. V. (1980), Numerical Heat Transfer and Fluid Flow, Hemisphere, New York.

Patzwahl, R., J. A. Jankowski, and T. Lege (2008), Very high resolution numerical modelling for inland waterway design, in Proceedings of the International Conference on Fluvial Hydraulics (River Flow 2008), IAHR, Izmir, Turkey.

Phillips, N. A. (1957), A coordinate system having some special advantages for numerical forecasting, J. Meteorol., 14, 184–185, doi:10.1175/1520-0469(1957)014<0184:ACSHSS>2.0.CO;2.

Prandtl, L. (1925), Bericht €uber Untersuchungen zur ausgebildeten Turbulenz, Z. Angew. Math. Mech., 5, 136–139.

Rodi, W. (1984), Turbulence Models and Their Application in Hydraulics, 104 pp., Int. Assoc. for Hydraulic Res., Delft, Netherlands.

Seo, J. H., and R. Mittal (2011), A sharp-interface immersed boundary method with improved mass conservation and reduced spurious pressure oscillations, J. Comput. Phys., 230, 7347–7363, doi:10.1016/j.jcp.2011.06.003.

Song, Y. T., and Y. Chao (2000), An embedded bottom boundary layer formulation for z-coordinate ocean models, J. Atmos. Oceanic Technol., 17, 546–560, doi:10.1175/1520-0426(2000)017<0546:AEBBLF>2.0.CO;2.

Stelling, G. S. (1995), Compact differencing for stratified free surface flow, in Advances in Hydro-Science and Engineering, vol. 2, Part A,

edited by the Chinese Hydr. Eng. Soc. pp. 378–386, Tsinghua University Press, Beijing, China.

Stelling, G. S., and J. van Kester (1994), On the approximation of horizontal gradients in sigma coordinates for bathymetry with steep bottom slope, Int. J. Numer. Methods Fluids, 18, 915–935, doi:10.1002/fld.1650181003.

Tseng, Y.-H., and J. H. Ferziger (2003), A ghost-cell immersed boundary method for flow in complex geometry, J. Comput. Phys., 192(2), 593–623, doi:10.1016/j.jcp.2003.07.024.

van Kester, J. (1994), Validatie Delft3D voor menglaag proef, Tech. Rep. Z810, WL | Delft Hydraul, Delft, Netherlands.

Wilcox, D. (1993), Turbulence Modeling for CFD, DCW Industries, La Ca~nada, Cali.

Wu, W., W. Rodi, and T. Wenka (2000), 3D numerical modeling of flow and sediment transport in open channels, J. Hydraul. Eng., 126(1), 4–15, doi:10.1061/(ASCE)0733-9429(2000)126:1(4).